Weierstraß-Institut
für Angewandte Analysis und Stochastik

Leibniz-Institut im Forschungsverbund Berlin e. V.

Preprint ISSN 2198-5855

Numerical simulation of high-frequency induction welding in longitudinal welded tubes

John Inge Asperheim[1], Prerana Das[1], Bjørnar Grande[1], Dietmar Hömberg[2],

Thomas Petzold[3]

submitted: June 14, 2019

[1] EFD Induction A.s
Bøleveien 10
3724 Skien
Norway
E-Mail: jia@no.efdgroup.net
bgr@no.efdgroup.net
Prerana.Das@efd-induction.com

[2] Weierstrass Institute
Mohrenstr. 39
10117 Berlin
Germany
E-Mail: dietmar.hoemberg@wias-berlin.de

[3] inpro
Innovationsgesellschaft für fortgeschrittene
Produktionssysteme in der Fahrzeugindustrie mbH
Steinplatz 2
10623 Berlin
E-Mail: Thomas.Petzold@inpro.de

No. 2600
Berlin 2019

2010 *Mathematics Subject Classification.* 35K05, 35Q61, 65N30.

Key words and phrases. Simulation, multi-field problem, Joule heating, welding.

This project has received funding from the European Union's Horizon 2020 research and innovation programme under the Marie Skłodowska-Curie grant agreement No. 675715.

Edited by
Weierstraß-Institut für Angewandte Analysis und Stochastik (WIAS)
Leibniz-Institut im Forschungsverbund Berlin e. V.
Mohrenstraße 39
10117 Berlin
Germany

Fax: +49 30 20372-303
E-Mail: preprint@wias-berlin.de
World Wide Web: http://www.wias-berlin.de/

Numerical simulation of high-frequency induction welding in longitudinal welded tubes

John Inge Asperheim, Prerana Das, Bjørnar Grande, Dietmar Hömberg, Thomas Petzold

Abstract

In the present paper the high-frequency induction (HFI) welding process is studied numerically. The mathematical model comprises a harmonic vector potential formulation of the Maxwell equations and a quasi-static, convection dominated heat equation coupled through the joule heat term and nonlinear constitutive relations. Its main novelties are twofold: A new analytic approach permits to compute a spatially varying feed velocity depending on the angle of the Vee-opening and additional spring-back effects. Moreover, a numerical stabilization approach for the finite element discretization allows to consider realistic weld-line speeds and thus a fairly comprehensive three-dimensional simulation of the tube welding process.

1 Introduction

High-frequency induction welding is widely used, especially in the production of superior quality oil and gas pipes and structural tubes. A steel strip is cold-formed into a tubular shape in a continuous roll forming mill. The strip edges are electromagnetically heated and joined mechanically by pushing the strip edges against each other to form the longitudinally welded tube (Figure 1).

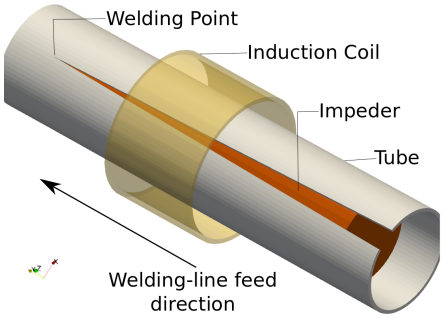

Figure 1: High Frequency induction welding of steel tube.

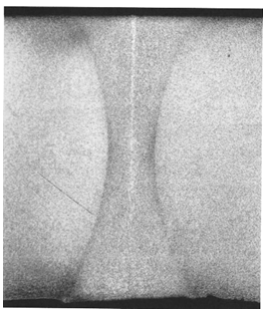

Figure 2: Macrograph of weld seam in tube cross-section.

The welded joint as seen in the transverse cross-section of a welded tube (Figure 2), is a very narrow zone compared to the tube diameter. The strip edges are heated to almost melting temperature and are pushed against each other in the viscoplastic state to form the welded joint where crystallographic texture and microstructural changes appear. It can be divided into three zones namely base metal, thermomechanically affected zone (TMAZ) and heat affected zone (HAZ). The transition zone between the base metal and HAZ is the TMAZ. In the HAZ, solid-solid phase transitions occur because of rapid temperature changes. These microstructural changes lead to change of mechanical properties in the HAZ. The characteristics of the HAZ depend heavily on how the tube and pipe manufacturer

DOI 10.20347/WIAS.PREPRINT.2600 Berlin 2019

set up the welding line and how the welding machine is being used.

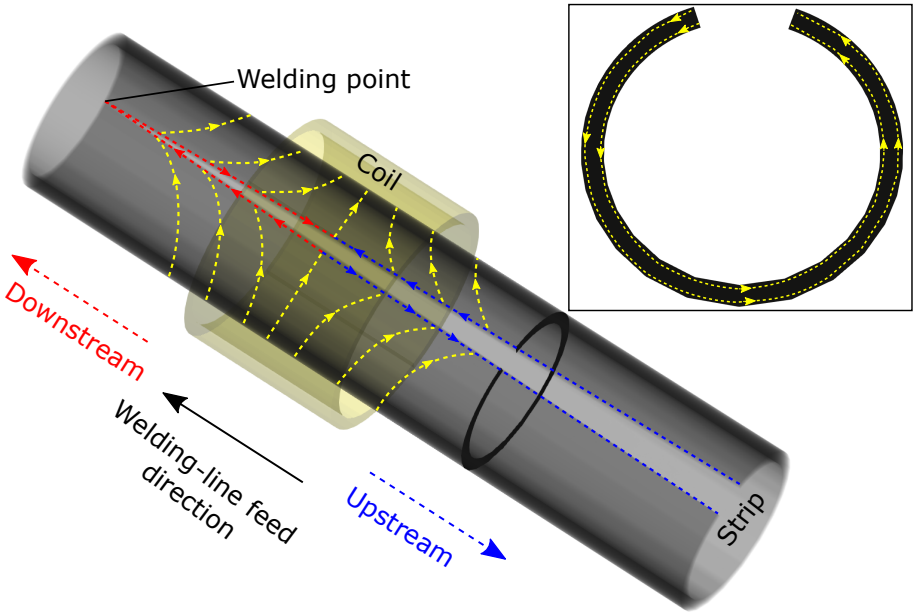

Figure 3: Schematic current path in the tube.

The electromagnetic heating of the tube is analogous to transformer theory. The coil is the primary current source, the strip is where the current is induced and the impeder acts as a magnetic core. The entire setup, coil current and frequency determine the amount of induced current in the tube.

High-frequency alternating current is supplied to the induction coil. This induces eddy currents in the strip under the coil. The induced current can follow the principal paths indicated in Figure 3 to complete the circuit. Along the strip edges, it can flow downstream from the coil towards the welding point or away from the coil in the upstream direction. At any strip cross-section, the current can follow a path either along the outer circumference or the inner circumference. The goal of high-frequency induction welding is to maximize the current density in the strip edge downstream, towards the welding point.

The impeder has a high relative magnetic permeability and guides the magnetic flux inside the formed strip. Thereby, the amount of current in the inner circumference of the strip to complete the circuit is reduced. Hence, the relative positioning of the strip, induction coil and impeder is very important to obtain an efficient heating process. Another factor which can affect the current concentration in the strip edges is the proximity of the strip edges to each other. The geometric shape of the opening between the strip edges is usually a Vee shape. Sometimes the Vee shape is distorted by spring-back due to the mechanical forming of the strip. This also affects the current distribution.

Further important process parameters are the coil current and welder frequency. The coil current is directly related to the power needed to obtain the desired temperature at the welding point. This would be in accordance with the required welding-line feed velocity for a given combination of tube diameter and wall thickness. Welder frequency is mainly based on what is required by the overall welding process, taking into account the tube/pipe product range, the available space for the impeder and the specified production rate. The choice of frequency is also influenced by considerations regarding the characteristics of the HAZ.

For better understanding of the complex interactions between the above parameters, numerical simulation is an indispensable tool. One of the earliest studies was by Scott [1], where the two-dimensional

(2D) heat equation is numerically solved and analytical formula is obtained for the power density in the tube in terms of some of the operating parameters. Parametric study on the Vee-angle, spring-back, weld speed and frequency with relative temperature distribution has been carried out in 2D for example, by Asperheim et al. [2]. A simplified three-dimensional (3D) numerical study of the HF welding was done by Lessmann et al. [3]. Jürgens et al. [4] also proposed a 3D FEM model but this had convergency problems with iterative solution process for high welding-feed velocities. One of the most recent 3D simulation approaches has been proposed by Nikanorov et al.[5]. All of these papers have in common that they have to make severe assumptions with respect to geometry or process data like welding-line speeds, which is not used in common practice.

In this paper we present the first comprehensive simulation approach for high-frequency induction welding in 3D. Its main novelties are twofold, a new analytic expression for the space-dependent velocity of tubes accounting for arbitrary Vee-angle and spring-back. In addition, we utilize a stabilization strategy which allows us to consider realistic welding-line speeds.

The outline of the paper is as follows: In Section 2 we describe the mathematical model based on a harmonic vector potential formulation of the Maxwell equations and a nonlinear heat equation. We derive an analytic characterization for a spatially varying tube velocity depending on the Vee-opening and spring-back and its influence on the system of equations. In Section 3, the approach to the numerical solution is discussed. Results of the simulations are presented in Section 4.

2 Mathematical model of induction welding

The high-frequency induction welding of steel tubes occurs in two stages: electromagnetic heating followed by mechanical joining of the tube edges. It is a multi-physics problem because of the electromagnetic, thermal, mechanical and metallurgical phenomena taking place during the process. Here, we focus only on the electromagnetic heating which is characterized by a coupling of the Maxwell equations with the heat equation. The welding of the tube is a part of a continuously moving production line. Hence, we will consider a quasi-stationary model.

2.1 Geometry

Figure 4 shows the different components considered for the electromagnetic heating of the tube. The formed steel strip and tube make up the workpiece, denoted as Ω_t. Until the welding point, it is the formed steel strip. After the welding point, it is assumed that the strip edges join to form the tube. The induction coil Ω_c is the non-contact electromagnetic heat source which heats the workpiece. Impeder Ω_i is a cylindrical solid structure made of an electrically non-conductive material with high magnetic permeability and acts as a magnetic flux concentrator. It is placed inside the formed strip, very close to the inner circumference of the strip. Its length extends until the welding point and ensures the concentration of current on the tube edges and prevents the current from closing the loop on the inside surface strip. The hold-all domain is defined as $\Omega = \Omega_t \cup \Omega_i \cup \Omega_c \cup \Omega_a$, where Ω_a is the surrounding air.

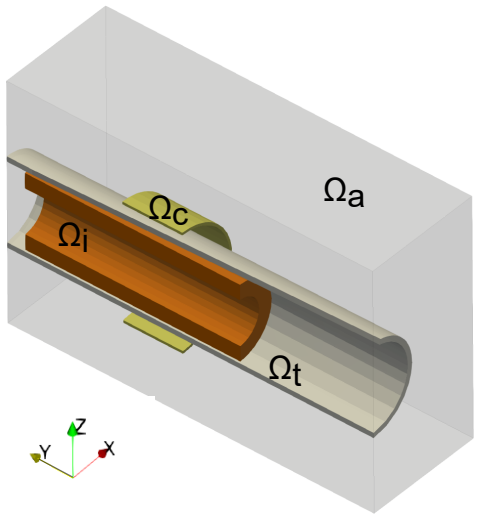

Figure 4: Weld setup for electromagnetic heating.

The strip geometry needs to be described such that it represents the forming of the strip during induction welding. The shape of the strip opening before the tube edges join at the welding point is an important factor that influences the welding. Ideally, it should appear as a "Vee" with a very narrow Vee-angle as shown in Figures 4 and 5(left). But effects like the spring-back effect can cause a distortion of the Vee shape, see Figure 5 (right). A parametrized geometry description for Ω_t will be given in Subsection 2.3. It is needed as a basis for the numerical simulations, moreover we will see that the deviation from a cylindrical shape leads to spatially varying feed velocity.

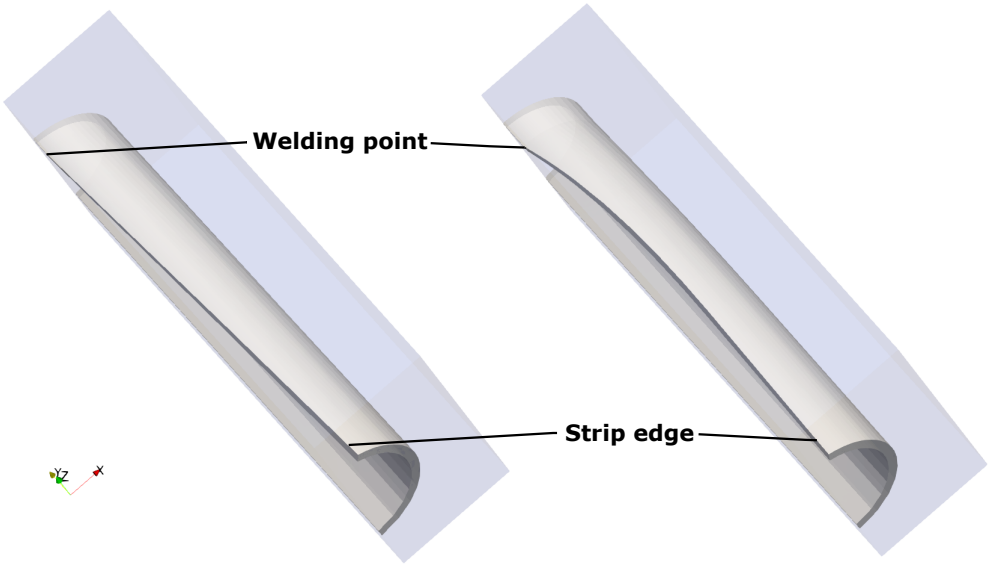

Figure 5: Variations of tube opening.

2.2 Electromagnetic induction heating problem

The problem domain is shown in Figure 4. The problem is defined in a time-harmonic regime where electric and magnetic fields are coupled. Alternating current is supplied in the coil, Ω_c which generates a magnetic field around the coil. The time-varying magnetic field induces an electric field creating eddy

currents in the electrically conductive steel tube, Ω_t. The impeder, Ω_i is used to control the path of the current in the tube. It is made of non-conducting material with high magnetic permeability. The surrounding air, Ω_a is also considered in the model.

We describe high-frequency welding by the time-harmonic Maxwell equations. To this end, we assume that all the fields behave periodically with respect to time with the same frequency ω and all fields are complex-valued. In eddy current problems, the displacement current is neglected. Hence, the harmonic Maxwell equations are given as follows,

$$\begin{aligned} \operatorname{curl} \mathbf{E} + i\omega\mathbf{B} &= 0 && \text{(1a)} \\ \operatorname{div}(\mathbf{B}) &= 0 && \text{(1b)} \\ \operatorname{curl} \mathbf{H} &= \mathbf{J}. && \text{(1c)} \end{aligned}$$

Here, $\mathbf{E}$ $[V/m]$ is the electric field, $\mathbf{B}$ $[Vs/m^2]$ magnetic flux density, $\mathbf{H}$ $[A/m]$ magnetic field, $\mathbf{J}$ $[A/m^2]$ current density and $\mathbf{E}$ $[V/m]$ the electric field. The system is completed by using the constitutive law. We assume

$$\mathbf{B} = \mu\mathbf{H}. \tag{2}$$

Here, $\mu[H/m]$ is the magnetic permeability which is material dependent and may be tensorial in nature. To account for a conductor moving with a relative velocity $\mathbf{v}$ Ohm's law has to be rewritten as

$$\mathbf{J} = \sigma(\mathbf{E} + \mathbf{v} \times \mathbf{B}). \tag{3}$$

In view of (1b) we introduce the magnetic vector potential $\mathbf{A}$ such that

$$\mathbf{B} = \operatorname{curl} \mathbf{A}. \tag{4}$$

Since $\mathbf{A}$ is not uniquely defined by this relation we impose in addition the Coulomb gauge $\operatorname{div} \mathbf{A} = 0$. Using (1a) and (4) we define the scalar potential ϕ by

$$\mathbf{E} + i\omega\mathbf{A} = -\nabla\phi. \tag{5}$$

Together with Ohm's law (3) we obtain the following expression for the total current density

$$J = -\sigma i\omega\mathbf{A} + \mathbf{v} \times \operatorname{curl} \mathbf{A} + \mathbf{J_{ext}}. \tag{6}$$

Here, the first term represents the eddy currents and the last one the impressed source current, which lives only in the induction coil Ω_c and is given by

$$\mathbf{J_{ext}} = -\sigma\nabla\phi. \tag{7}$$

Now, we utilize (1c) to obtain the vector potential formulation of the Maxwell equations (1),

$$\sigma(i\omega\mathbf{A} - v \times \operatorname{curl} \mathbf{A}) + \operatorname{curl}\left(\frac{1}{\mu} \operatorname{curl} \mathbf{A}\right) = \mathbf{J_{ext}}. \tag{8}$$

In Section 2.4 we will show that the velocity term $v \times \operatorname{curl} \mathbf{A}$ can actually be neglected for typical weld-line speeds. Therefore, the final partial differential equation for the time-harmonic Maxwell's equation in vector potential formulation is given by

$$\sigma i\omega\mathbf{A} + \operatorname{curl}\left(\frac{1}{\mu} \operatorname{curl} \mathbf{A}\right) = \mathbf{J_{ext}}. \tag{9}$$

We assume that the tangential component of the vector potential vanishes on the boundary $\partial\Omega$, i.e., we define

$$\mathbf{A} \times \mathbf{n} = 0 \quad \text{on } \partial\Omega. \tag{10}$$

The source current $\mathbf{J_{ext}}$ as defined in (7) can be precomputed analytically. To this end we assume that the coil is a toroid with rectangular cross-section, where r_o and r_i are the outer and inner radius, and h is the height. Then assuming continuity for the source current, we demand $\operatorname{div}(\sigma\nabla\phi) = 0$. In cylindrical coordinates, we obtain

$$\phi = C_1\varphi \quad \text{and consequently } \mathbf{J_{ext}} = \sigma C_1\,(0, 1/r, 0)^T_{(r,\varphi,z)}$$

where $C_1 = U_0/(2\pi)$ for a given voltage. For a given source current in the coil, C_1 is computed from

$$\int_\Gamma \mathbf{J_{ext}} \cdot \tilde{n}\,\mathrm{da} = I_{\text{coil}}.$$

In Cartesian coordinates the source current is then given as

$$\mathbf{J_{ext}} = I_{\text{coil}}\frac{\log(r_i/r_o)}{h}\begin{pmatrix} -y/(x^2+y^2) \\ x/(x^2+y^2) \\ 0 \end{pmatrix}. \tag{11}$$

Next we consider the thermal part of the problem. The aim of the simulation is to find the temperature distribution in the tube. Hence, only the strip and tube is considered in the thermal part of the simulation. The heat distribution in the tube is determined from the quasi-stationary convection-diffusion equation for heat transport,

$$c_p\rho\boldsymbol{v}\cdot\nabla\theta - \operatorname{div}\lambda\nabla\theta = Q_{src}. \tag{12}$$

Here, θ is the temperature [°C] , $c_p\rho$ [$Jm^{-3}K^{-1}$]is the volumetric heat capacity and λ [$Wm^{-1}K^{-1}$] is the thermal conductivity. Q_{src} [Jm^{-3}] denotes the volumetric heat source.The term $\boldsymbol{v}\cdot\nabla\theta$ represents the transport of the temperature field with $\boldsymbol{v}$ [ms^{-1}] denoting the velocity of the tube. With this modification of the heat equation, the movement of the tube is taken into account, and we will see in Section 2.4 that in contrast to the Maxwell system here the velocity term cannot be neglected.
We have to complement the heat equation with boundary conditions on $\partial\Omega_t$. We distinguish three different parts of the tube boundary, two faces and the lateral surface. At the strip inlet face the temperature is assumed to be at room temperature. Hence a Dirichlet boundary condition of 25°C is assigned here. On the tube outlet face we assume a homogeneous Neumann condition. On the lateral surface a Robin boundary condition is prescribed, i.e.,

$$-\lambda\nabla\theta\cdot\mathbf{n} = h(\theta-\theta_0). \tag{13}$$

Here, h denotes the heat transfer coefficient between the tube and air, and θ_0 is the surrounding temperature.

2.3 Tube parametrization and spatially varying velocity

As we have seen already, the strip is bended until it finally becomes a tube at the welding point, see Figure 5. To parametrize the domain, we assume that the centerline of the tube coincides with the y-axis, such that cross-sections with $y < 0$ correspond to circular cross-sections with (outer) tube

radius r_t. We assume that half the size of the tube opening is measured by a prescribed function $w(y)$, such that $w(y) = 0$ for $y \leq 0$. It allows to describe arbitrary strip openings including spring back (see Figure 5, right). We assume that for $y > 0$ the bended strip is already of circular shape with a radius $r(y)$ and (half) an opening angle $\phi(y)$, both depending on the width of the strip opening $w(y)$ (see Figure 6).

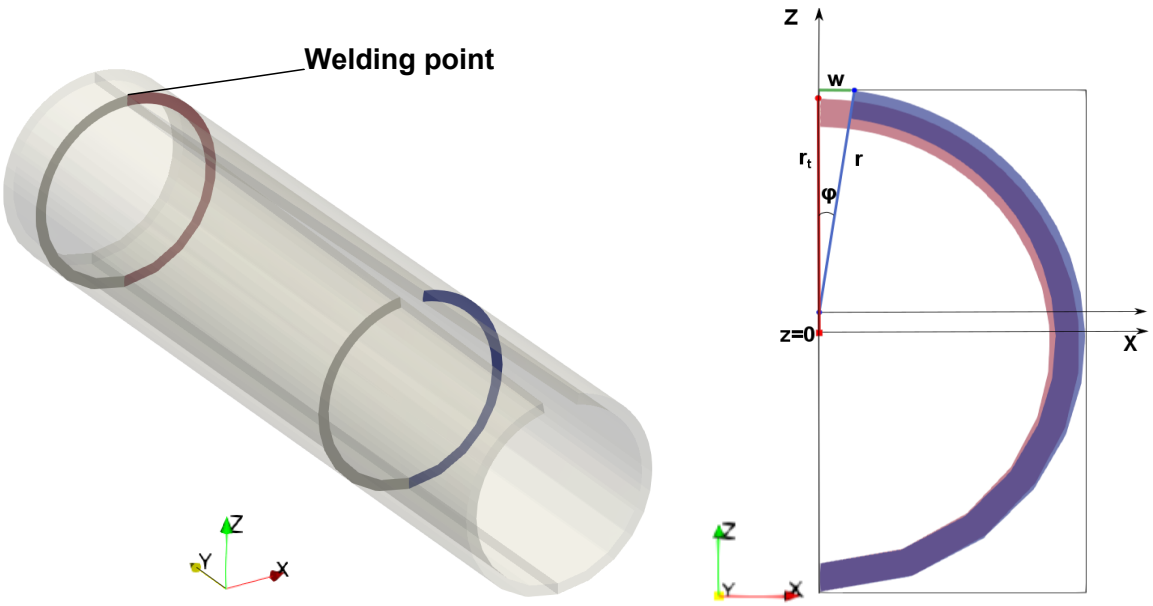

Figure 6: Parameterization of strip geometry

More precisely, we can characterize $r(y)$ and $\phi(y)$ as the solution the nonlinear system

$$(\pi - \phi(y))r(y) = \pi r_t \tag{14a}$$

$$w(y) = r(y)\sin\phi(y). \tag{14b}$$

A solution can only be found numerically. To this end, we we fix $N > 0$ and define equidistant nodes $y_i = i\frac{y_{max}}{N}$, $i = 0, \ldots N$. Note that $\phi_0 = \phi(y_0) = 0$. Then for $1 \leq i \leq N$ we compute $\phi_i = \phi(y_i)$ by applying Newtons method to solve

$$f_i(\phi) = \frac{\pi r_t \sin\phi}{(\pi - \phi)} - w(y_i)$$

where we choose the result at the previous node as the initial value for the next one. Then, we apply cubic spline interpolation to obtain a smooth function $\phi(y)$, $y \in [0, y_{max}]$ and use (14a) to obtain $r(y)$ (see Figure 7), i.e.

$$r(y) = \frac{\pi r_t}{\pi - \phi(y)}.$$

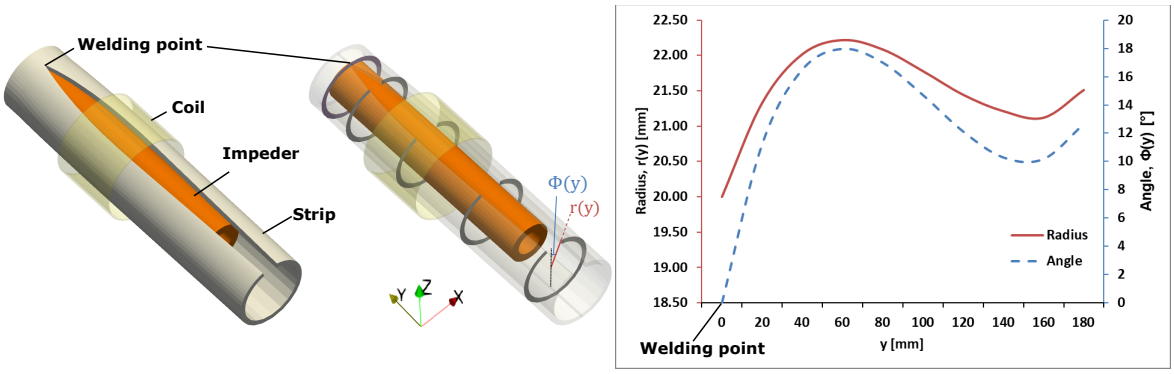

Figure 7: Functions: $r(y)$ and $\phi(y)$.

Now we are in a position to parameterize the tube domain using cylindrical coordinates with respect to the y-axis. Note that in view of (14a) for a fixed cross-section $y \in [0, y_{max}]$, $r(y)$ is the outer radius and $(\pi - \phi(y))r(y)$ the arc length of the open tube arc. Hence, for a tube of wall thickness h, any point in the tube at cross-section y can be described as

$$\vec{X}(y, \alpha, \rho) = \begin{bmatrix} (r(y) + (\rho - 1)h)\, \sin\left(\alpha \dfrac{\pi - \varphi(y)}{\pi}\right) \\ y \\ (r(y) + (\rho - 1)h)\, \cos\left(\alpha \dfrac{\pi - \varphi(y)}{\pi}\right) + r(y) - r_t \end{bmatrix}. \tag{15}$$

Here, $\rho \in [0, 1]$ defines a radial location between outer ($\rho = 1$) and inner tube radius ($\rho = 0$), and $\alpha \in [0, \pi]$ is the angular position between opening edge ($\alpha = 0$) and tube botton ($\alpha = \pi$). This parametrization allows for an easy computation of the locally varying velocity. After the welding point is reached the the velocity has only a component in the feeding direction y, while before the velocity varies locally with non-vanishing radial and angular components. To obtain the correct temperatures especially close to the strip edge it is crucial to use the correct locally varying velocity for the simulation.

To this end we consider the trajectory of a point in a tube cross-section moving with constant weld-speed v, i.e.

$$g(t) = \vec{X}(y_{max} - vt, \alpha, \rho) \tag{16}$$

with velocity

$$\dot{g}(t) = -v \frac{\partial \vec{X}}{\partial y}(y, \alpha, \rho) \tag{17}$$

and

$$\frac{\partial \vec{X}}{\partial y}(y, \alpha, \rho) = \begin{bmatrix} \dfrac{\partial}{\partial y}\left((r(y) + (\rho - 1)h)\, \sin\left(\alpha \dfrac{\pi - \varphi(y)}{\pi}\right)\right) \\ 1 \\ \dfrac{\partial}{\partial y}\left((r(y) + (\rho - 1)h)\, \cos\left(\alpha \dfrac{\pi - \varphi(y)}{\pi}\right) + r(y) - r_t\right) \end{bmatrix}. \tag{18}$$

Figure 8 shows the resulting local velocity vectors for selected points on the strip opening for a spring back tube opening. Instead of a constant velocity solely in y-direction one can see that now the velocity follows the contour of the opening.

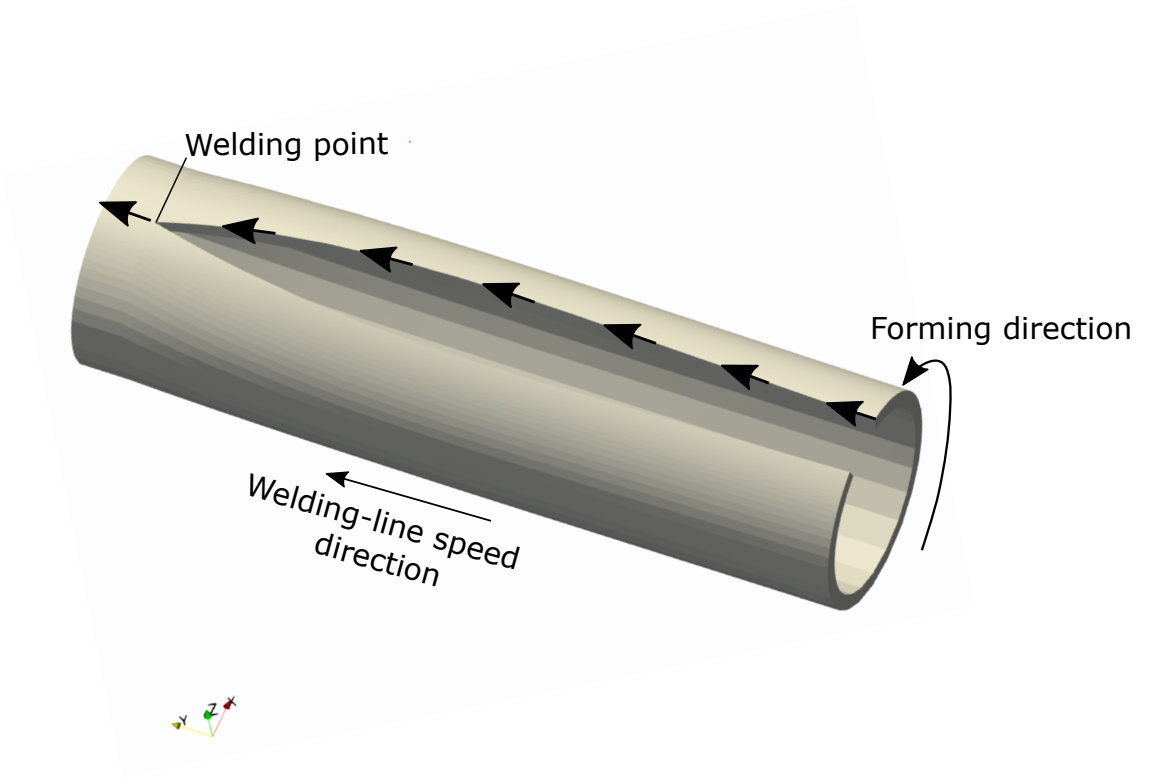

Figure 8: Local velocity to represent feed velocity and forming.

2.4 Non-dimensionalization of governing equations

In this subsection we analyze the influence of tube movement on the solutions of the Maxwell system and the heat equation, respectively. Consider first the time-harmonic Maxwell equations in vector potential formulation,

$$\sigma(i\omega\mathbf{A} \; - \; v \; \times \; \mathrm{curl}\,\mathbf{A}) \; + \; \mathrm{curl}\,\frac{1}{\mu}\;\mathrm{curl}\;\mathbf{A} = \mathbf{J_{ext}}. \tag{19}$$

Substituting variables for non-dimensionalization, i.e. $x = L\tilde{x}$ and the magnetic potential vector to be $\mathbf{A} = A_0\tilde{\mathbf{A}}$.

$$i\tilde{\mathbf{A}} \; - \; \frac{v}{L\omega} \times \; -\tilde{\mathrm{curl}}\tilde{\mathbf{A}} \; + \; \frac{1}{L^2\mu\sigma\omega}\,\tilde{\mathrm{curl}}\,\tilde{\mathrm{curl}}\,\mathbf{A} = \frac{\mathbf{J_{ext}}}{A_0\sigma\omega}. \tag{20}$$

The term $i\tilde{\mathbf{A}}$ indicates the induced current and $\frac{v}{L\omega} \times \; \mathrm{curl}\,\tilde{\mathbf{A}}$ denotes the induced current due to movement. Consider length scale L to be the penetration depth. The numerical value of the factor $\frac{v}{L\omega}$ when calculated for high-frequency welding of steel ($L = 1 \times 10^{-3}m$ and $\omega = 100 \times 10^3 s^{-1}$) is of the order of 10^{-2}. Hence, the current induced due to the movement can be neglected for HFI tube welding simulation.
Fourier's heat equation with convection is given by equation (12).

$$c_p\rho\,\boldsymbol{v}\cdot\nabla\theta - \mathrm{div}\,\lambda\nabla\theta = Q_{src}. \tag{21}$$

Introducing the non-dimensional constants for length as $x = L_* \, \tilde{x}$ and temperature $\theta = \Theta \, \tilde{\theta}$, equation (21) can be rewritten by,

$$\frac{c_p \rho \boldsymbol{v} L}{\lambda} \, \tilde{\nabla} \tilde{\theta} - \tilde{\nabla}^2 \tilde{\theta} = \frac{L^2}{\lambda \Theta} \, Q_{src}. \tag{22}$$

Here, the Péclet number is given by the coefficient, $\frac{c_p \rho \boldsymbol{v} L}{\lambda}$. If the Péclet number is greater than 1, then this will cause a significant oscillation in the temperature. Indeed, for typical welding-line speeds and materials data for carbon steels it takes values ranging in the interval $[12, 26]$. Hence, the influence of the heat transport term during the electromagnetic heating simulation cannot be neglected.

3 Numerical solution

3.1 System parameters and material data

Low-carbon steel is one of the most commonly used materials for manufacturing welded steel tubes. In the present work, non-linear material properties of steel strip have been considered. The electrical conductivity and thermal conductivity are shown in Figure 9 which is for low-carbon steel [6].

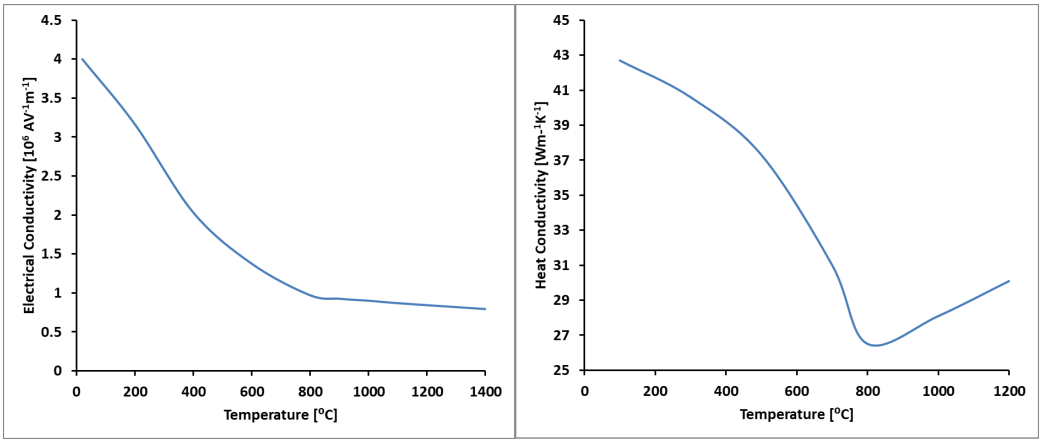

Figure 9: Electrical and thermal conductivity of low-carbon steel.

For the volumetric heat capacity and the definition of magnetization we use parametrized curves as described in [7]. Note that these include a number of parameters which have been identified for induction heating processes in a costly process. They are confidential and cannot be disclosed by EFD Induction A.s., but similar data can be found in literature, cf., e.g., [8]. For the volumetric heat capacity we consider

$$\rho \, C_p(T) \; = \; \rho \, C_{Pi} \; + \; (\rho \, C_{P0} - \rho \, C_{Pi}) e^{-\frac{T}{\tau}} \; + \; E \, g(T) \tag{23a}$$

$$g(T) \; = \; \frac{1}{\sigma \sqrt{2\pi}} e^{\frac{1}{2}\left(\frac{T - T_c}{\sigma}\right)^2} \tag{23b}$$

with constants $\rho \, C_{p0}$, $\rho \, C_{Pi}$, E, σ, T_c, and τ. The formula for magnetic flux density is given by (24)

$$B(H,T) \;\; = \;\; \mu_0 \, H \; + \; \frac{2 J_{s0}}{\pi} \, \gamma(T) \arctan\left(\frac{\pi(\mu_{r0} - 1) \, \mu_0 \, H}{2 J_{s0} \, . \, \gamma}(T) \right) \tag{24a}$$

$$\gamma(T) \;\; = \;\; \frac{1 - e^{\frac{T - T_c}{C}}}{1 - e^{-\frac{T_c}{C}}} \tag{24b}$$

with constants μ_0, μ_{r0}, J_{s0}, T_c, and C. The geometry of the strip and the setup of the coil and impeder is created based on standard setup rules used in a real welding station. The main input parameters for the setup are the diameter, thickness and Vee-angle or Vee-opening of the strip. The FEM simulations are carried out for two circular cross-section tubes of different sizes. The welder frequency for induction heating is set at 250 kHz. The welding-line feed velocity is 100m/min. The current supply I_{coil} is selected depending on the final desired temperature in the strip edge. For the simulations, the current supply is set such that the temperature at the welding point in mid-thickness reaches 1250℃.

	Tube 1	**Tube 2**
Tube Radius, r_t	20 mm	11 mm
Tube Thickness, h	3 mm	1 mm
Coil Radius	25 mm	14 mm
Coil Thickness	3 mm	1 mm
Impeder Radius	12 mm	10 mm
Impeder Thickness	5 mm	3 mm
Vee-opening	$3°$, $5°$, $7°$, Spring-back	
Frequency	250 kHz	
Welding-line speed	100 m/min	

Table 1: Simulation parameters

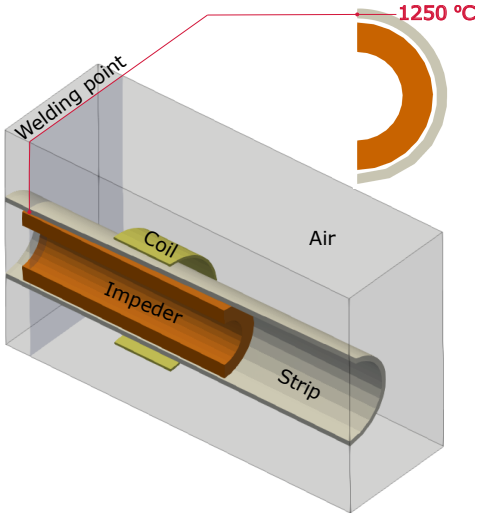

Figure 10: Weld setup for current controlled simulations.

3.2 Discretization and solution strategy

The electromagnetic heating is governed by Maxwell's equation in the time-harmonic regime (9) and the quasistationary heat equation with transport (12). To reduce the computational effort we only consider one half of the domain, cf. Figure 10, hence additional symmetry boundary conditions have to be added at this artificial boundary.

The computational mesh is generated by the grid generator TetGen [9] and the coupled system is solved using the C++ library pdelib, a finite element toolbox developed at WIAS.

The heat equation is discretized by linear nodal finite elements. The heat in the tube is generated by the effect of Joule heat from the eddy currents induced. This heat is distributed by diffusion. The tube itself is not stationary but moving, which also causes convective transport of heat. The tubes in the welding-line move at very high speeds somewhere in the range of 40m/min to 200 m/min. As we have remarked earlier, in this range the Péclet number is greater than 1, it means that the process is convection dominated. When using the Galerkin Finite Element method, as Péclet number increases, the solution has a sharp gradient and fails to capture the non-linear solution accurately[10]. To stabilize the solution, we utilize the Streamline Upwind Petrov Galerkin (SUPG) method, which adds a residual based stabilization term to the finite element formulation [11]. It uses a stabilization parameter which is a function of the local Péclet number, the local velocity and the mesh size and is also referred to as the intrinsic time scale.

In contrast to temperature, where continuity across element boundaries holds, for the magnetic vector potential A continuity across elements can only be expected in tangential direction, in normal direction

discontinuities might occur. To this end we follow [8] and use lowest order Nédélec elements for the discretization of the vector potential equation (9). The magnetization depends both on the temperature and the magnetic field (24). For fixed temperature this nonlinearity is resolved numerically based on an averaging approach. For details we refer again to [8].

Finally, the coupled system is iteratively decoupled and solved using a fixed point iteration as depicted in Figure 11.

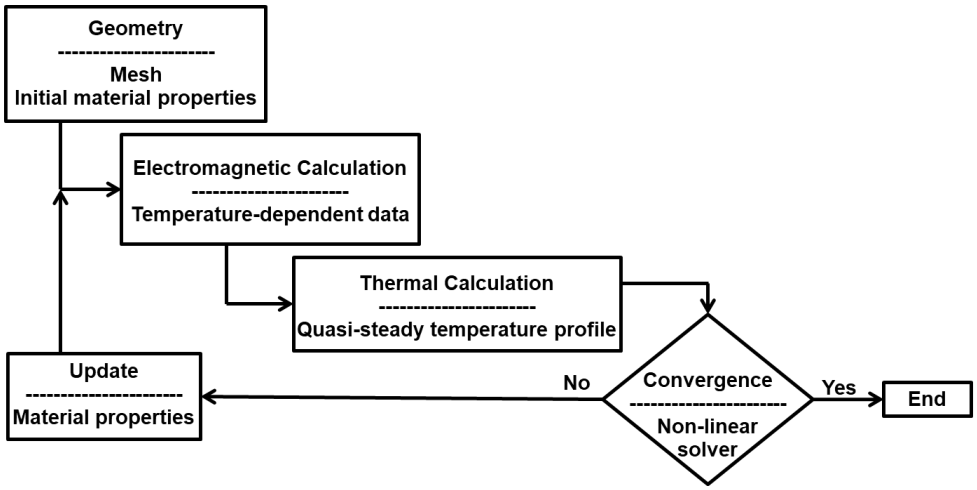

Figure 11: Simulation flowchart.

4 Results

For a better visibility most of the results are shown for tube 1, i.e. for the bigger tube diameter. Examples of temperature distribution in the welded strip are shown in Figure 12. The strip edges are heated to very high temperatures because of Joule heating from eddy current concentration.

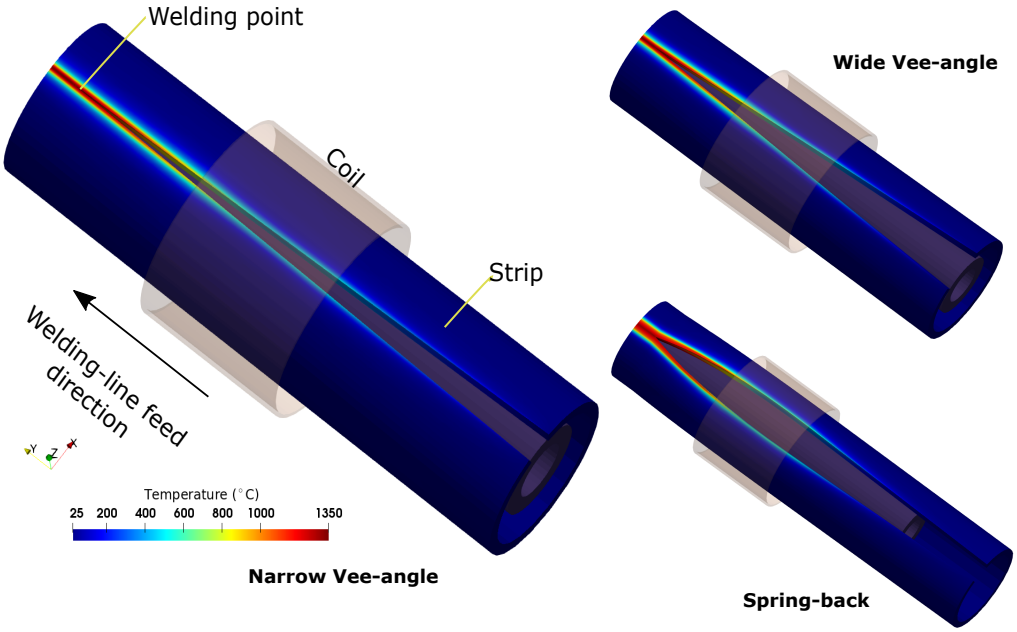

Figure 12: Temperature distribution in the tube.

In the simulations, a spatially dependent velocity is used as explained in Section 2.3. Figure 13 shows the comparison of temperature distribution results in case of the model with constant velocity to that of the model with spatially varying velocity. It is seen that the temperature profile follows the spring-back shape of the strip in the case where spatially varying velocity function is used.

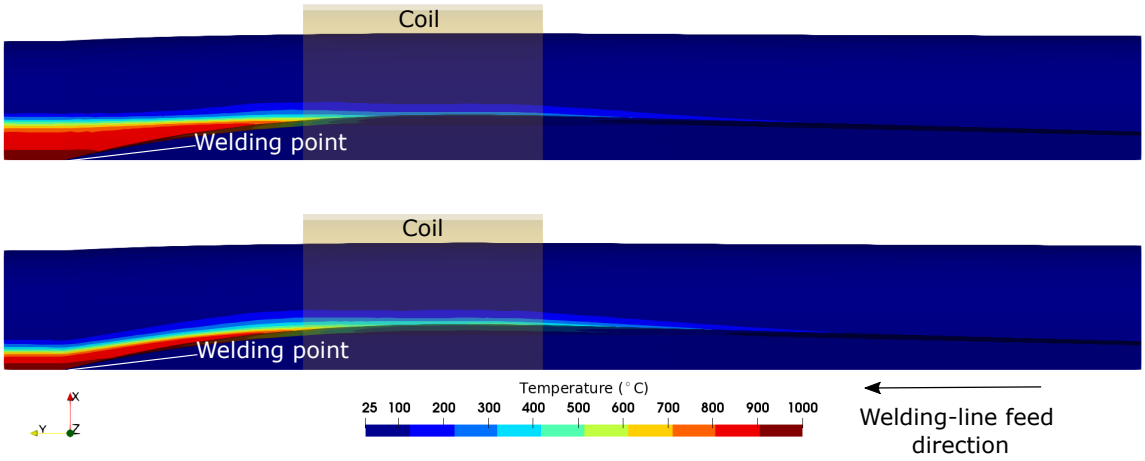

Figure 13: Temperature distribution of model with constant velocity (top) and model with spatially varying velocity (bottom).

Figure 14 shows some of the magnetic field lines. It is seen that the magnetic flux is directed through the impeder. At the strip and tube boundaries with the Dirichlet condition, the magnetic field is contained in the welding station.

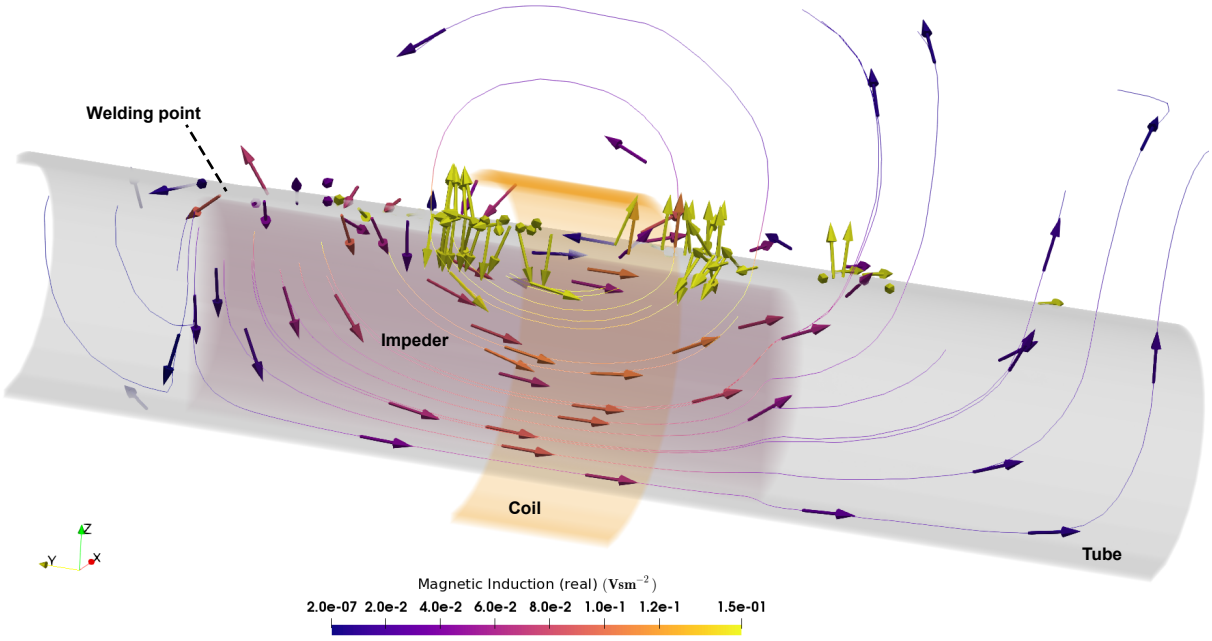

Figure 14: Magnetic field lines during electromagnetic induction.

A simulation result of current density distribution in the strip edge is shown in Figure 15. It shows current concentration both in the downstream and upstream directions. As explained in Section 1, the principal current paths are already well-known based on general understanding of magnetic field and

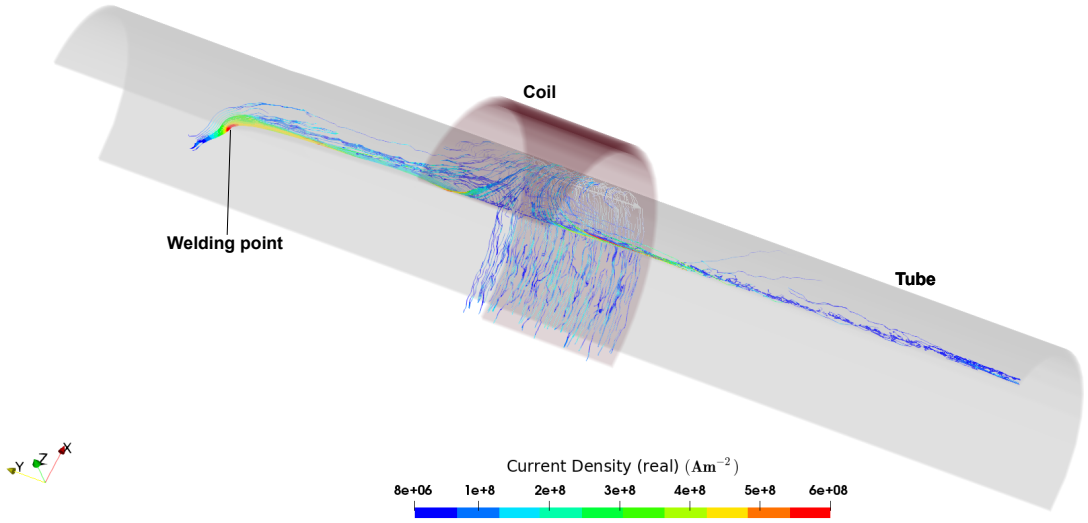

Figure 15: Current path in the tube.

current. With the developed model, it is possible to quantify the different current levels in the principal current paths (Figure 15). For closer investigation of the current in different paths, models with four different domain boundaries corresponding to cross-sections $\Gamma_{14},\ \Gamma_{12},\ \Gamma_{11},\ \Gamma_7$ are considered (Figure 16). In these models (tube radius, r_t = 20mm), the strip lengths beyond the impeder in the upstream direction are given in Table 2. The longitudinal current at different cross-sections ($\Gamma_1,\ \Gamma_2, ...,\ \Gamma_{14}$) of the strip is calculated from equation (25).

Domain boundary	Relative upstream strip length beyond impeder
Γ_{14}	$12\,r_t$
Γ_{12}	$4\,r_t$
Γ_{11}	$3\,r_t$
Γ_7	$0.7\,r_t$

Table 2: Models with different domain boundaries.

$$I_{\Gamma_i} = \int_{\Gamma_i} \mathbf{J} \cdot \mathbf{n}\,\mathrm{d}A \qquad \{i \in \mathbb{N} \quad 1 \leq i \leq 14\}. \tag{25}$$

In the table of Figure 16, the current of equation (25) is expressed as a percentage of the external coil current ($\mathbf{J_{ext}}$). Ideally, we would like to have a model where the current at the upstream domain boundary is almost nil. This is seen in the simulation result of the model with domain boundary at Γ_{14}. Because the model length is very long, the mesh quality maybe compromised. Hence, we try to choose a model with shorter strip length but similar current levels in the different cross-sections ($\Gamma_1, \Gamma_2, ..., \Gamma_7$). It is seen that the current levels in the model with domain boundary at Γ_{12} matches most closely to those of model with domain boundary at Γ_{14}. Hence, this model's upstream domain boundary length i.e. $4\,r_t$ has been used for the test case, Tube 1 (Table 1).

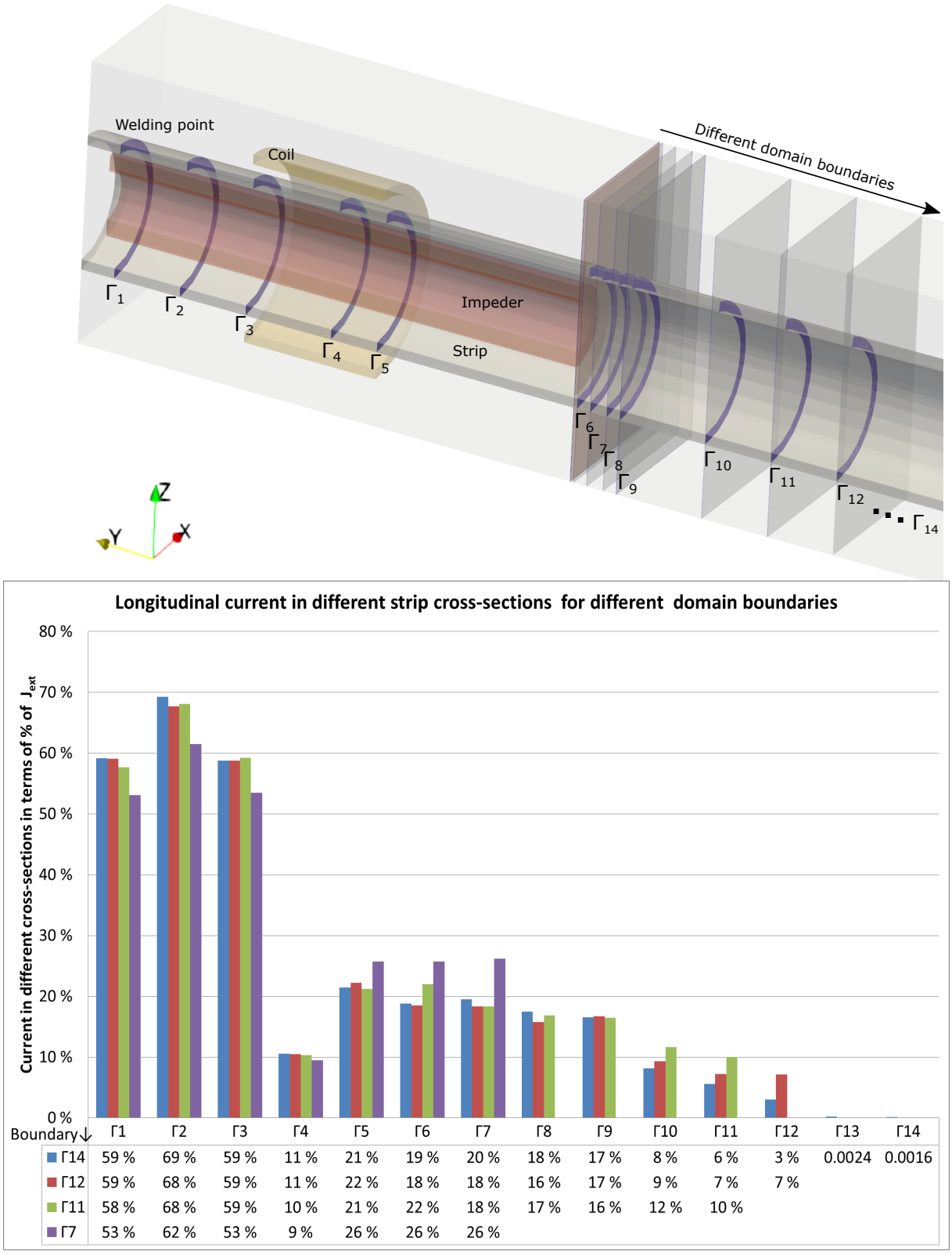

Boundary ↓	Γ1	Γ2	Γ3	Γ4	Γ5	Γ6	Γ7	Γ8	Γ9	Γ10	Γ11	Γ12	Γ13	Γ14
Γ14	59 %	69 %	59 %	11 %	21 %	19 %	20 %	18 %	17 %	8 %	6 %	3 %	0.0024	0.0016
Γ12	59 %	68 %	59 %	11 %	22 %	18 %	18 %	16 %	17 %	9 %	7 %	7 %		
Γ11	58 %	68 %	59 %	10 %	21 %	22 %	18 %	17 %	16 %	12 %	10 %			
Γ7	53 %	62 %	53 %	9 %	26 %	26 %	26 %							

Figure 16: Current in Y-direction in different strip cross-sections (slices).

The division of current path in the upstream and downstream directions is also reflected in consequent temperatures in the strip edge in Figure 17. The temperature drops midway of the coil because of the currents dividing in the two opposite directions.

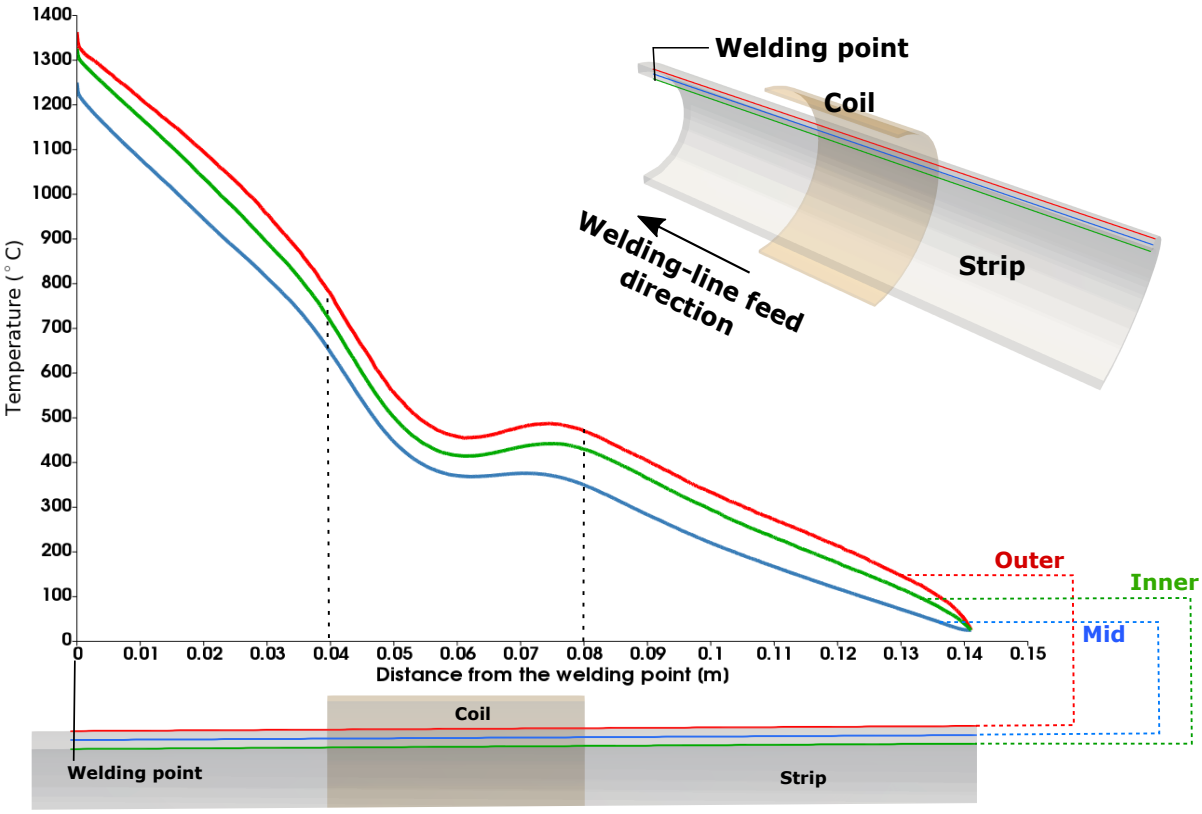

Figure 17: Temperature in the strip edge.

Figure 18 shows the temperature for different cross-sections in the strip. It is seen that the temperature profile in the strip edge has an hourglass shape. This is related to the current distribution in the cross-section of the strip edges. The current distribution is influenced by the current penetration depth, the geometry of the strip edges and the position of the impeder. The temperature distribution is also a result of thermal conduction in the strip cross-section where power generation and heat transfer take place.

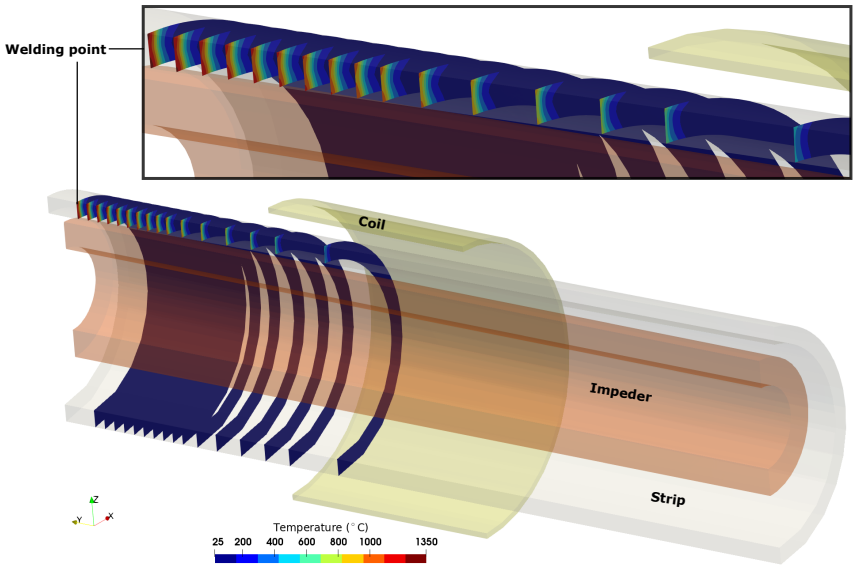

Figure 18: Evolution of temperature profile in the strip edge towards welding point.

The heat affected zone at the welding point is shown for two different tube dimensions in Figure 19. The hourglass shape is more pronounced in case of thicker tubes. At the welding point, the temperature of the strip edge at the outer circumference and inner circumference may differ depending on the closeness of the impeder to the inner circumference. When the distance between the impeder and the inner circumference of the strip is large, the magnetic field lines are spread out in this gap before concentrating into the impeder. This causes more heating of the strip edges at the inner circumference. When the impeder is close enough to the inner circumference of the strip, most of the magnetic field lines are directed more vertically out of the gap between the two strip edges, with less heating of the corners at the inner circumference as the result. However there are physical limitations of how small the gap between the impeder and the inner circumference of the strip can be.

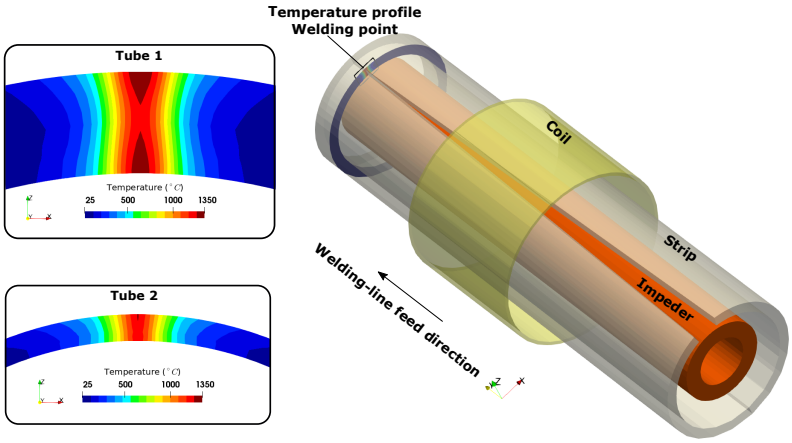

Figure 19: Heat Affected Zone at welding point for different tube dimensions.

5 Conclusions

A three-dimensional model has been developed for high-frequency induction welding. It is a non-linearly coupled system of Maxwell's electromagnetic equation and the heat equation. The system equations are discretized by FEM and solved using the fixed point iteration based on an incremental decoupling. The model includes the use of non-linear magnetic and thermal material properties. The model also considers the high welding-line velocities which accounts for the heating by advection and conduction in the strip. The results show temperature distribution in the strip edges that develops as expected from previous studies and visual observations of the process. First, the corners of the strip are heated and as the welding point approaches the characteristic hour glass shape of the heat affected zone is formed. The boundary conditions at the strip and tube ends are considered to be Dirichlet conditions as it represents the process correctly. The strip length used in the model also decides the amount of induced current that goes to the welding point. For the thinner wall tube, the hour glass shape of heat affected zone is less pronounced. This is in line with what is expected from literature. The observations from the results are dimension specific and not necessarily the same for tubes of other dimensions.

This new three-dimensional simulation tool will provide a basis for an optimization of the design of the welder, especially with respect to the dimensioning of induction coil,impeder and the configuration of these relative to the steel strip. Future work will include the study of the mechanics of the material squeeze-out when the strip edges are joined together after heating.

References

[1] P. F. Scott. „Key parameters of High Frequency Welding“. In: *Tube International* March (1996), pp. 1–17.

[2] J. I. Asperheim and B. Grande. „Temperature Evaluation of Weld Vee Geometry and Performance“. In: *Tube International* 19 (2000), pp. 497–502.

[3] H.-J. Lessman, A Muiznieks, and G Seefried. „Optimisation of Longitudinal Induction Welding of Tubes“. In: *Tube & Pipe Technology* (Sept. 2003), pp. 83–87.

[4] R. Jürgens, U. Ludtke, and D. Schulze. „Three-dimensional calculation of the distribution of eddy currents and the heating effect on slit tubes when welding longitudinal seams“. In: *IEEE Transactions on Magnetics* 30 (5 Sept. 1994), pp. 3705–3708. DOI: 10.1109/20.312746.

[5] A. Nikanorov et al. „Approaches for numerical simulation of high frequency tube welding process“. In: *Proc of Int'l Sci Colloq Modelling for Electromagnetic Processing (MEP2014)*. Hannover, Germany, Sept. 2014, pp. 445–450.

[6] J. Davies and P. Simpson. *Induction Heating Handbook*. McGRAW-HILL Book Company(UK) Limited, 1979.

[7] Cedrat. *Flux - electromagnetic and thermal finite element software*. 2015. URL: http://www.cedrat.com/en/software/flux.html.

[8] D. Hömberg et al. „Simulation of multi-frequency-induction-hardening including phase transition and mechanical effects“. In: *Finite Element Analysis Design* 200 (June 2016), pp. 86–100. DOI: 10.1016/j.finel.2016.07.012.

[9] H. Si. „TetGen, a Delaunay-Based Quality Tetrahedral Mesh Generator“. In: *ACM Trans. Math. Softw.* 41.2 (Feb. 2015), 11:1–11:36. ISSN: 0098-3500. DOI: 10.1145/2629697. URL: http://doi.acm.org/10.1145/2629697.

[10] J. Donea and A. Heuerta. *Finite Element Methods for Flow Problems*. John Wiley and Sons, 2003.

[11] V. John, P. Knobloch, and S. Savescu. „A posteriori optimization of parameters in stabilized methods for convection-diffusion problems-Part I“. In: *Computer Methods in Applied Mechanics and Engineering* 200 (Oct. 2011). DOI: 10.1016/j.cma.2011.04.016.